Chinese Chemical Letters 34 (2023) 107891

Contents lists available at ScienceDirect

Chinese Chemical Letters

journal homepage: www.elsevier.com/locate/cclet

Sequentially responsive size reduction and drug release of core-satellite nanoparticles to enhance tumor penetration and effective tumor suppression

Jiayi Sun[a], Jingyang Li[a], Xi Li[b], Lu Yang[a], Yitong Liu[c,*], Huile Gao[d], Li Xiang[a,*]

[a] State Key Laboratory of Southwestern Chinese Medicine Resources, Innovative Institute of Chinese Medicine and Pharmacy, Chengdu University of Traditional Chinese Medicine, Chengdu 611137, China
[b] Public Health Clinical Center of Chengdu, Chengdu 610061, China
[c] The Third Affiliated Hospital of Chengdu University of TCM/Chengdu Pidu District Hospital of Traditional Chinese Medicine, Chengdu 611730, China
[d] West China School of Pharmacy, Sichuan University, Chengdu 610041, China

ARTICLE INFO

Article history:
Received 6 August 2022
Revised 6 October 2022
Accepted 7 October 2022
Available online 13 October 2022

Keywords:
Size reducible
Tumor penetration
Core-satellite structure
Mesoporous silica nanoparticles
Gold nanoclusters
Experimental techniques

ABSTRACT

Poor tumor accumulation remains a serious challenge for nanomedicines to achieve ideal antitumor outcomes. The different size preferences for systematic circulation, tumor retention and deep permeation have attracted great attention when designing antineoplastic nano-delivery system. Herein, we developed a nano-system which can shrink its size in tumor microenvironment to achieve better tumor retention and penetration. In this work, the cationic bovine serum albumin-protected, doxorubicin-loaded gold nanoclusters (CAuNC-DOX) and amino-functionalized mesoporous silica nanoparticles (MSN) are connected by Fe^{2+} and are further coated with hyaluronic acid (HA) to obtain a core-satellite MSN-Fe-CAuNC-DOX@HA nano system (MFADH). When reaching the tumor site, the HA shell, which endows the system with both good biocompatibility and preferable tumor targeting ability, was disintegrated, followed by acid-stimulated release of small-sized pharmacological unit—CAuNC-DOX for further tumor penetration. As demonstrated in both *in vitro* and *in vivo* results, MFADH showed excellent antitumor effect, providing a proof of concept for the feasibility of shrinkable nanoplatforms in tumor treatment.

Nanoplatform based drug delivery systems have sparked great interest due to its ability in improving tumor targeting, bioavailability and efficacy of chemotherapeutics [1]. However, the delivery efficacy has severely impaired due to the complex tumor environment such as high interstitial fluid pressure and abnormal vasculature [2–4]. Numerous researches have revealed that the size of nanomedicine largely dictates their biodistribution, tumor penetration, and systematic clearance, thus affecting overall therapeutic efficacy against cancers [5,6]. Small-sized nanoparticles (less than 30–50 nm) were believed to exhibit better tumor penetration compared with their large counterparts [7–10], but they also suffered from insufficient tumor accumulation due to rapid systematic clearance [11]. By comparison, relatively large-sized ones (60–200 nm) showed optimal passive tumor targeting ability by utilizing both enhanced permeability and retention (EPR) effect and prolongated circulation [12–15]. Considering all above-mentioned ingredients, shrinkable nano-systems that can transformed from the original large size to smaller ones in response to tumor microenvironment (pH, enzymes, light and *etc.*) have been widely proposed [16–21]. This strategy can solve the dilemma between circulation, penetration and accumulation, which not only endows the integrated nano-system with longer blood circulation and suitable size for EPR effect, but also allows the shrunken nanoparticles to penetrate deep in tumor, so as to improve drug delivery efficiency and antitumor effect [14].

Bovine serum albumin protected gold nanoclusters (AuNC@BSA) with several nanometers possess good biocompatibility and red fluorescence, and are easy to conjugate drugs on the surface, which are commonly served as tracer carriers for cancer therapy [22]. Recent researches confirmed that the cationic AuNC@BSA (CAuNC) has high drug-loading capacity and tumor permeability, resulting in efficient drug delivery in tumor [23]. CAuNC has abundant amino groups on the surface, so it can be coupled with the antitumor drug doxorubicin (DOX) to form doxorubicin-loaded CAuNC

* Corresponding authors.
E-mail addresses: Liuxsc1989@126.com (Y. Liu), xianglydr@cdutcm.edu.cn (L. Xiang).

https://doi.org/10.1016/j.cclet.2022.107891
1001-8417/

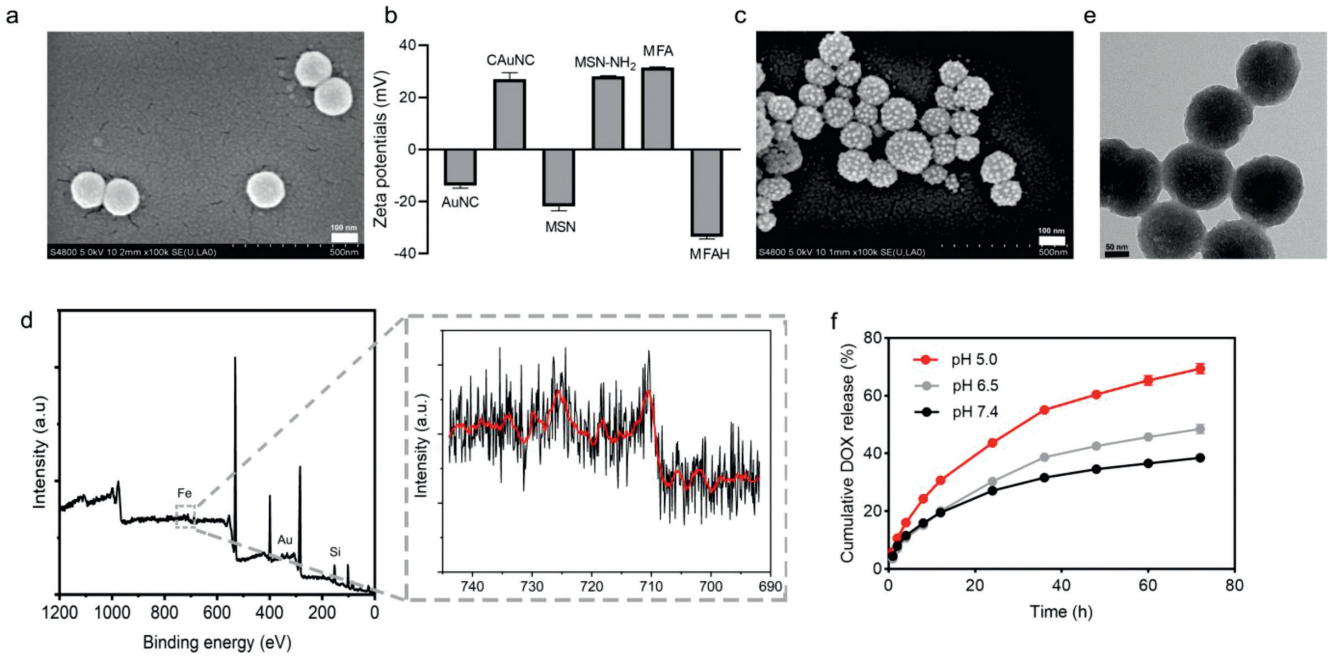

Fig. 1. The characterization of MFADH. (a) SEM images of MSN-NH_2 (Scale bar: 100 nm). (b) Zeta potentials of different nanoparticles. (c) SEM images of MFA (Scale bar: 100 nm). (d) XPS image of MFA and the characteristic peak of Fe. (e) TEM image of MFAH (Scale bar: 50 nm). (f) Cumulative DOX release curve of CAuNC-DOX in pH 5.0, pH 6.5 and pH 7.4 in 72 h.

(CAuNC-DOX) by acid-responsive hydrazone bond, which allow the DOX released in acidic tumor microenvironment to exert antitumor effect. However, individual CAuNC can be quickly cleared from bloodstream due to the small size. To extend the blood circulation time, CAuNC could be carried on larger platform to increase the size so as to reduce the renal clearance.

Mesoporous silica nanoparticles (MSN) have high specific surface area, controllable particle size, good biocompatibility and can be easily modified on the surface [24,25]. Functionalized MSN has been shown to responded to various stimuli to release drugs, such as pH, redox, enzyme and light [26–28], which endow functioned MSN the ability to realize stimuli responsive of CAuNC. Since Fe^{2+} can coordinate with amino groups under neutral conditions and dissociate under acidic conditions, we chose amino-functionalized MSN to link with CAuNC *via* Fe^{2+}.

Herein, we constructed a core-satellite structure nano-system MSN-Fe-CAuNC (MFA) composed of amino-functionalized MSN and CAuNC, in which Fe^{2+} served as the bridging ion coordinating with amino groups. The ion-ligand is sensitive to acidic pH [29], so that the core-satellite structure could disassociate in tumor microenvironment to achieve size reduction. To further improve blood circulation and tumor targeting, hyaluronic acid (HA), a negative charged ligand of CD44 receptor [30], which could also shield the positive charge of MFA and prevent non-specific protein adsorption, was introduced. When the HA-coated nanosystem MSN-Fe-CAuNC-DOX@HA (MFADH) arrived at tumor, HA was degraded by the over-expressed hyaluronidase in tumor microenvironment and MFAD was exposed. Then acidic tumor microenvironment triggered broken of the iron-amino coordination structure, and the small sized CAuNC-DOX was dissociated, which could penetrate deeply into the tumor and released DOX to improve the effectiveness of antitumor therapy.

MSN were prepared by a typical sol-gel process [31], and scanning electron microscopy (SEM) was applied to characterize the morphology of MSN and MSN-NH_2 (Fig. 1a and Fig. S1 in Supporting information). Both of them showed spherical morphology with uniform size. According to dynamic light scattering (DLS) analysis, the hydrodynamic diameter of MSN was 192.9 ± 6.1 nm (Fig. S2 in Supporting information). The zeta potential of MSN increased from −21.9 ± 1.7 mV to 28.1 ± 0.2 mV after amino-functionalized (Fig. 1b), indicating the successfully amino-modification of MSN. The hydrodynamic diameter of CAuNC was 17.67 ± 0.71 nm, and its zeta potential was 27.0 ± 2.5 mV. The red fluorescent emission suggested the successfully synthesis of CAuNC (Fig. S3 in Supporting information). The immobilization of CAuNC on the MSN-NH_2 with Fe^{2+} linker and the attached HA was extensively characterized. As shown in SEM images (Fig. 1c), the MFA NPs were spherical with a non-hydrodynamic size of approximately 150 nm, and presented a granular surface fully covered by individual CAuNC. X-ray photoelectron spectroscopy (XPS) of MFA showed characteristic peak of Fe, Au, Si (Fig. 1d), also manifested the MSN-NH_2 and CAuNCs were successfully linked by Fe^{2+}. The peaks at 711 eV and 725 eV indicated that both Fe^{2+} and Fe^{3+} existed in MFA, indicated that part of Fe^{2+} was oxidized to Fe^{3+} during the process of synthesis, so that the characteristic peak of Fe^{3+} also existed in the spectrum. The transmission electron microscopy (TEM) of MFAH showed lower electron density on the edge (Fig. 1e), which might cause by the adsorption of HA on the surface. The hydrodynamic diameter of MFA increased from 220.2 ± 6.12 nm to 237.9 ± 8.7 nm after the adsorption of HA, with the zeta potential changed from 31.5 ± 0.2 mV to −33.5 ± 0.9 mV, also represented the successfully synthesis of MFAH NPs.

DOX had a drug loading efficiency of 10.7% on CAuNC by covalently binding Shiff base reaction. The Schiff base bonds are unstable under acidic condition, so that DOX could release from CAuNC in acidic environment. As shown in Fig. 1f, the cumulative release of DOX was increased with time, and when the pH got lower, DOX released faster. In the condition of pH 5.0, approximately 70% DOX released from CAuNC in 72 h. However, in the condition of pH 7.4 and pH 6.5, only 38.5% and 48.5% DOX could release at the time point of 72 h, indicating that the release of DOX from CAuNC-DOX was both acid-response and time-dependent, which could reduce the side-effect of DOX but enhance the antitumor effect after internalized into tumor cells.

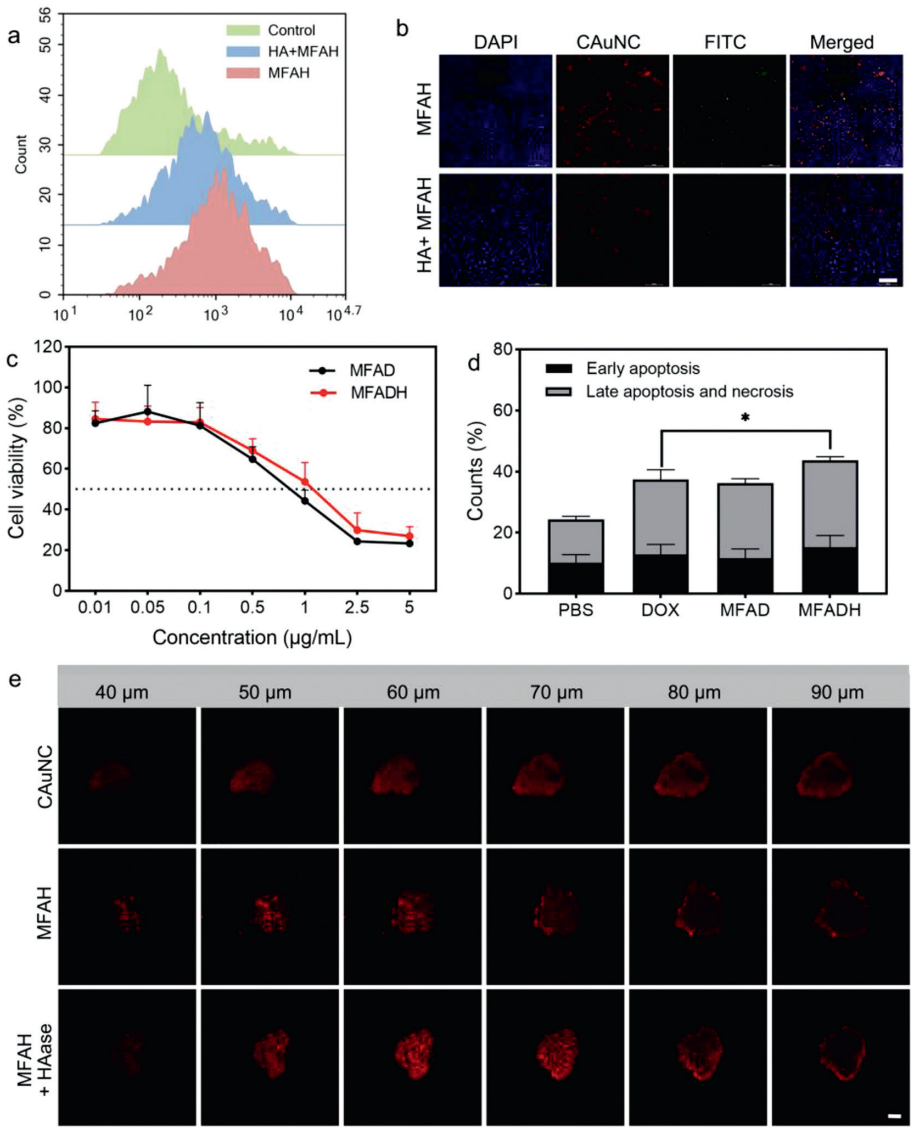

Fig. 2. (a) Cellular uptake of 4T1 after preincubated with or without HA followed by incubated with FITC-labeled MFAH, detected by flow cytometry. (b) CLSM images of cellular uptake of 4T1 after preincubated with or without HA followed by incubated with FITC-labeled MFAH (Scale bar: 100 nm). (c) Cytotoxicity of MFAD and MFADH on 4T1 cells, the concentration represents the loaded DOX in the preparations. (d) Flow cytometric analysis of apoptotic cells after different treatments: PBS (blank), DOX, MFAD, MFADH. (e) Penetration of different nanoparticles into tumor spheroids (Scale bar: 100 nm).

To investigate the uptake activity of MFAH by 4T1 cells, FITC-labeled nanoparticles were incubated with 4T1 and HA-preincubated 4T1. The flow cytometry result showed HA-preincubated 4T1 cells internalized less FITC-labeled MFAH (Fig. 2a). That is because preincubation with HA could saturated the CD44 receptor, thus reducing the specific binding between CD44 and MFAH. The images of confocal laser scanning microscopy (CLSM) showed similar results (Fig. 2b).

Following this, the cytotoxicity of nanocarriers on RAW264.7 were detected by MTT assay. As showed in Fig. S4 (Supporting information), CAuNC and MSN-NH_2 showed no obvious toxicity to RAW264.7. However, the toxicity of MFA to RAW264.7 increased with increasing concentration, which probably due to the augment of iron ion in the nanoparticles. After coating by HA, MFAH reversed the toxicity, that might be attributed to the changed surface-charge of nanoparticles and the reduced iron ion release, suggesting that MFAH possess good biocompatibility. Then the cell viability and cell apoptosis of 4T1 was investigated. As shown in Fig. 2c, the cell viability of 4T1 decreased with the increase of preparation concentration, and both of the MFAD and MFADH showed high toxicity on 4T1 cells. Next the effect on cell apoptosis of the preparations. As shown in Fig. 2d, 4T1 treated with MFADH displayed higher apoptosis rate compared with free DOX, indicating that MFADH possessed better killing effect on 4T1 cells. These results preliminarily proved that MFADH had the ability to inhibit 4T1 cell growth.

Then the tumor spheroids penetration ability was detected by CLSM to confirm the size-reduced capacity of formulations. The CLSM images showed small-sized positively charged CAuNC could penetrate into tumor spheroids deeply (Fig. 2e), which displayed stronger fluorescence intensity in the spheroids than MFAH. However, after incubated with hyaluronidase, MFAH could penetrate much deeper and displayed stronger fluorescence intensity, and even comparable with CAuNC, demonstrated that hyaluronidase could degrade HA on the surface of MFAH and promote CAuNC disassociation from MSN, which considerably improved the penetration capacity.

Furthermore, the *in vivo* tumor-targeting ability and distribution of CAuNC and MFAH in 4T1-tumor bearing BALB/c mice were evaluated. The animal study was reviewed and approved by the

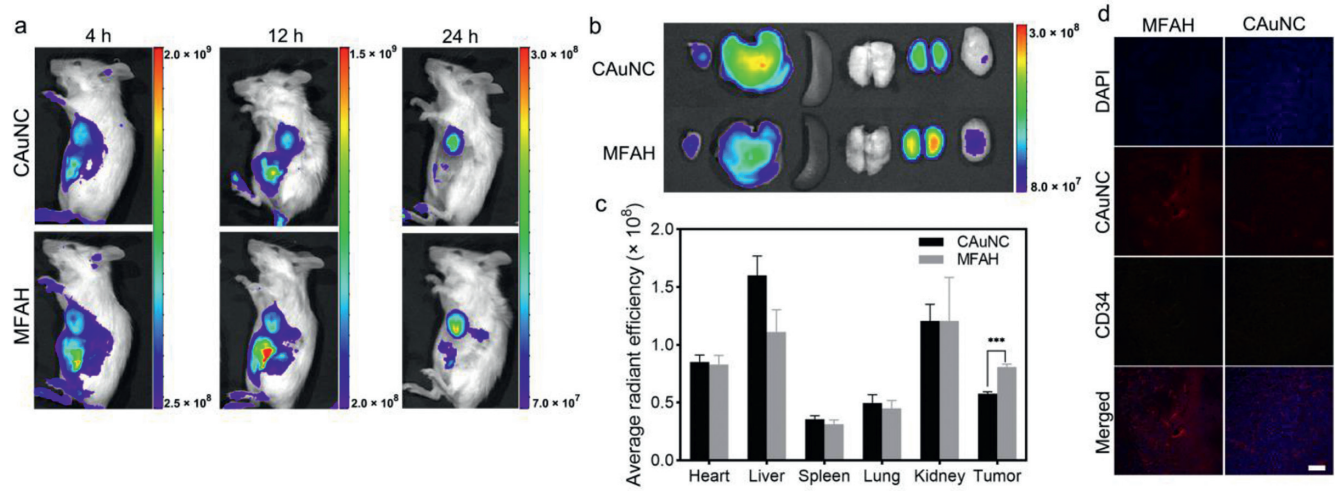

Fig. 3. *In vivo* distribution of CAuNC and MFAH. (a) *In vivo* fluorescent imaging of ICG signal at different time points, the unit of radiant efficiency is [(p/sec/cm^2/sr)/(μW/cm^2)]. (b) *Ex vivo* imaging of CAuNC signal of organs and tumors (left to right are respectively heart, liver, spleen, lung, kidneys and tumor). (c) Semi-quantification of average radiant efficiency of *ex vivo* organs and tumors. (d) The slices of *ex vivo* tumors imaged by CLSM, blue represents nucleus stained by DAPI, red represents the signal of CAuNC, and orange represents blood vessels marked by Cy3-conjugated anti-CD34 antibody. The scale bar represents 100 μm.

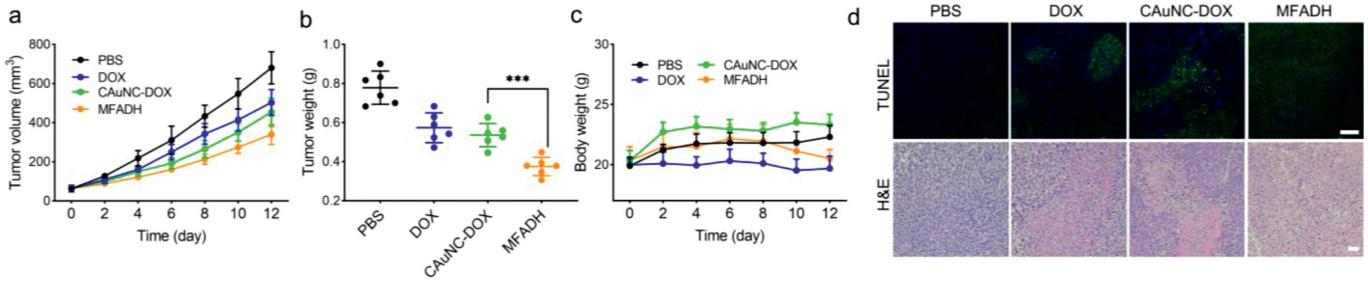

Fig. 4. *In vivo* antitumor efficacy investigation. (a) Tumor growth curves measured every 2 days. (b) Weights of *ex vivo* tumors. (c) Body weight curves measured every 2 days. (d) TUNEL and H&E staining of tumor slices. The scale bar represents 100 μm.

Institutional Animal Care and Use Committee (IACUC) of Chengdu University of Traditional Chinese Medicine. ICG was adsorbed with CAuNC and used for tracer to visualized nanoparticle distribution *in vivo*. As shown in Fig. 3a, both nanoparticles could target to tumor tissue. But under the same injected dose of ICG, the fluorescence signal in tumor site of MFAH NPs got stronger than that of CAuNC NPs, represented that MFAH NPs had better tumor retention efficacy in 24 h. The *ex vivo* images and the fluorescence semi-quantitative result displayed that CAuNC NPs had more distribution in liver and lung and less distribution in tumor compared with MFAH NPs (Figs. 3b and c). The same conclusion could be drawn from the slices of *ex vivo* tumors (Fig. 3d). The tumor slices from MFAH NPs group displayed stronger fluorescence than that of CAuNC NPs group, and the fluorescence not only distribute around the blood vessel, but also penetrate to other area. These results demonstrated the MFAH nanocarriers had considerable higher tumor-targeting accumulation, so they might enhance the bioavailability of loading drugs.

Finally, the antitumor effects of MFADH were evaluated in 4T1-tumor bearing BALB/c mice *in vivo*. As shown in Fig. 4a, the average tumor volume of mice in PBS group increased to 700 mm^3 at the end of the treatment. Without big size nanocarriers to delivery antitumor drugs, the groups of DOX and CAuNC-DOX showed certain therapeutic efficiency but not as well as the groups of MFADH group, which was consistent with the tumor weight showed in Fig. 4b. Changes in body weight of the mice could reflect the systemic toxicity of drugs. As shown in Fig. 4c, the mice of MFADH group got slightly body weight reduction during the treatment, however, the body weight of the mice in DOX group decreased faster than that of MFADH group, which corroborated that MFADH could reduce the toxicity of DOX. The TUNEL and H&E of tumor slices also confirmed that MFADH group had the highest tumor cell apoptosis and had the most prominent damage in the tumor tissue (Fig. 4d). The H&E of major organs indicated that BALB/c mice treated with MFADH showed no obvious histopathological damage in the major organs compared to the PBS treated mice (Fig. S5 in Supporting information), which proved that MFADH possessed ideal biological safety. All the result above indicated that MFADH had the possibility to inhibit tumor growth and the size reduction strategy could enhance the efficiency of drug delivery and improve antitumor effect.

In conclusion, a core-satellite structure MSN-Fe-CAuNC-DOX@HA was fabricated, which could sequentially respond to the tumor microenvironment and release small-sized CAuNC-DOX to increase drug penetration in the tumor. The prepared nanoparticles exhibited the ability to target to tumor cells, increase the accumulation of CAuNC in the tumor site, and the binding CAuNC could disassociate from MSN in response to the tumor microenvironment to increase the penetration depth, which achieved good antitumor effect *in vitro* and *in vivo*. Considering the fact that MFADH had good biocompatibility and antitumor efficacy, this size-reduced strategy has great potential to become a highly effective cancer treatment modality.

Declaration of competing interest

The authors declare that they have no known competing financial interests or personal relationships that could have appeared to influence the work reported in this paper.

Acknowledgment

This study was supported by Xinglin Scholar Research Premotion Project of Chengdu University of TCM (No. MPRC2021031).

Supplementary materials

Supplementary material associated with this article can be found, in the online version, at doi:10.1016/j.cclet.2022.107891.

References

[1] F.M. Kievit, M. Zhang, Adv. Mater. 23 (2011) H217–H247.
[2] Y. Zhou, X. Chen, J. Cao, H. Gao, J. Mater. Chem. B 8 (2020) 6765–6781.
[3] S. Yang, H. Gao, Pharmacol. Res. 126 (2017) 97–108.
[4] X. Gao, J. Zhang, Z. Huang, ACS Appl. Mater. Interfaces 9 (2017) 29457–29468.
[5] A. Schädlich, H. Caysa, T. Mueller, et al., ACS Nano 5 (2011) 8710–8720.
[6] M.I. Setyawati, C.Y. Tay, B.H. Bay, D.T. Leong, ACS Nano 11 (2017) 5020–5030.
[7] Y. Niu, J. Zhu, Y. Li, et al., J. Control. Release 277 (2018) 35–47.
[8] B. Su, R. Wang, Z. Xie, et al., Small 14 (2018) 1702331.
[9] J. Wang, W. Mao, L.L. Lock, et al., ACS Nano 9 (2015) 7195–7206.
[10] J. Hu, X. Yuan, F. Wang, et al., Chin. Chem. Lett. 32 (2021) 1341–1347.
[11] W. Yu, M. Shevtsov, X. Chen, H. Gao, Chin. Chem. Lett. 31 (2020) 1366–1374.
[12] C. Hu, X. Yang, R. Liu, et al., ACS Appl. Mater. Interfaces 10 (2018) 22571–22579.
[13] X. Cun, M. Li, S. Wang, et al., Nanoscale 10 (2018) 9935–9948.
[14] W. Yu, R. Liu, Y. Zhou, H. Gao, ACS Cent. Sci. 6 (2020) 100–116.
[15] Z. Shi, Q. Li, L. Mei, Chin. Chem. Lett. 31 (2020) 1345–1356.
[16] C. Hu, X. Cun, S. Ruan, et al., Biomaterials 168 (2018) 64–75.
[17] H. Li, J. Du, J. Liu, et al., ACS Nano 10 (2016) 6753–6761.
[18] R. Tong, H.H. Chiang, D.S. Kohane, Proc. Natl. Acad. Sci. U. S. A. 110 (2013) 19048–19053.
[19] J. Wang, S. Shen, J. Li, Z. Cao, X. Yang, ACS Nano 15 (2021) 4636–4646.
[20] W. Wu, Y. Pu, J. Shi, Adv. Sci. 8 (2021) 2002816.
[21] Z. Wang, Y. Wang, X. Sun, et al., Small 18 (2022) 2200588.
[22] R. Liu, W. Jia, Y. Wang, et al., Research 2022 (2022) 9847612.
[23] R. Liu, C. Hu, Y. Yang, J. Zhang, H. Gao, Acta Pharm. Sin. B 9 (2019) 410–420.
[24] Y. Zhou, G. Quan, Q. Wu, et al., Acta Pharm. Sin. B 8 (2018) 165–177.
[25] A. García-Fernández, F. Sancenón, R. Martínez-Máñez, Adv. Drug Deliv. Rev. 177 (2021) 113953.
[26] Q. Lei, W. Qiu, J. Hu, et al., Small 12 (2016) 4286–4298.
[27] Z. Luo, K. Cai, Y. Hu, et al., Angew. Chem. Int. Ed. 50 (2011) 640–643.
[28] J. Hu, D. Xiao, X. Zhang, Small 12 (2016) 3344–3359.
[29] R. Jin, Z. Liu, Y. Bai, et al., Adv. Funct. Mater. 28 (2018) 1801961.
[30] Z. Luo, Y. Dai, H. Gao, Acta Pharm. Sin. B 9 (2019) 1099–1112.
[31] F. Tang, L. Li, D. Chen, Adv. Mater. 24 (2012) 1504–1534.